Influence of the tip-induced electric field on the STM contrast of chemisorbed C_2H_4 on the Si(001) surface

H. Ness and A. J. Fisher
Department of Physics and Astronomy, University College London, Gower Street, London WC1E 6BT, United Kingdom
(Received 2 October 1996; revised manuscript received 9 December 1996)

We present a first-principles calculation for the Si(001) surface on which ethylene molecules (C_2H_4) are adsorbed. The calculations apply the recently developed projector-augmented-wave method together with the Car-Parrinello scheme to determine the ground-state atomic and electronic structures. It is shown that the scanning tunneling microscopy (STM) contrast observed experimentally for this surface cannot be understood by considering only the surface wave functions obtained in zero electric field. The tip-induced electric field strongly modifies the surface electronic structure. A detailed study of the polarization of the Si(001) surface with and without adsorbed C_2H_4 molecules is presented. Given the direction of the electric field, the electronic charge is ''pulled out'' from the surface into the vacuum. The response of the electronic states to the electric field is greater above the clean silicon dimers than above the molecules. Constant-current STM scans are obtained from a nonperturbative approach to the calculation of the tunneling current. In the presence of the tip-induced electric field, the resulting STM contrast is found to be in qualitative agreement with the experiments. [S0163-1829(97)08615-3]

I. INTRODUCTION

Scanning tunneling microscopy (STM) (Ref. 1) is now a well-established tool for probing conducting surfaces and obtaining real-space images of such surfaces at the atomic scale. A number of studies have been performed on silicon surfaces and more especially on the reconstruction of the Si(001) surface.[2] Futhermore there have been a number of studies concerning the interaction of small organic molecules (such as acetylene, ethylene, propylene) with silicon surfaces. Such studies are important for the understanding of the adsorption mechanisms as well as for practical applications (e.g., silicon carbide films obtained by chemical vapor deposition). For example, a recent study performed by Mayne *et al.* concerns the chemisorption of ethylene (C_2H_4) on the Si(001) (2×1) surface.[3] STM images of both the filled and empty states have been obtained. A detailed analysis of these images led to the identification of the surface dimers, the adsorbed molecules and other surface defects.[4] In particular, it was shown that the C_2H_4 molecules appear slightly darker than the clean silicon dimers when tunneling out of the surface (e.g., in the STM images corresponding to the surface filled states). At first sight the fact that the molecules deposited on the Si(001) (2×1) surface appear darker than the bare dimers themselves is surprising.

However it is now well recognized that STM images are influenced not only by the atomic structure at the surface, but also by the atomic and electronic structure of the whole tunneling junction (i.e., the sample surface, the adsorbates if any are present, and the tip). In principle the tunneling current between the tip and the sample is dependent on the individual electronic structure of both the tip and the surface and also on the tip-sample interaction, in the sense that the presence of the tip close to the surface should modify the electronic structure of both systems. Several authors have pointed out that when the tip and the sample interact strongly (i.e., when the tip is sufficiently close to the surface to form a kind of bonding with it), the electronic and atomic structures of both the tip and the surface can be highly distorted. This can lead to images which cannot be understood in the context of the Tersoff-Hamann approximation.[5] For example, Doyen *et al.* have shown that such a strong tip-sample interaction can lead to contrast inversion in STM images of metallic surfaces.[6] It should also be noticed that there is another class of problems for which the STM images cannot always be described within the Tersoff-Hamann approximation. This is when the tip-sample current tunnels via some particular adsorbed species on the sample surface, as for example in Ref. 7.

However, even when the tip-sample distances are such that the tip-sample bonding is small, some other effects have a crucial role. For example, the tip-induced electric field, long ranged as compared to the tip-sample bonding, may have a non-negligible influence on the electronic structure of the sample surface. This is especially so on semiconductors, for which a finite bias has to be applied before any tunneling can take place. The influence of an external electric field on the electronic structure of surfaces has already been studied by a number of workers. For example, Lam and Needs have studied the screening of electric fields at the Al(111) and Al(001) surfaces,[8] Neugebauer and Scheffler have investigated the adsorption-desorption of alkali (Na,K) atoms on the Al(111) surface,[9] Huang *et al.* have analyzed the electronic charge polarization of the Si(001) surface due to the tip-induced electric field,[10] and more recently, Hirose and Tsukada have developed a model to study a STM-like junction under strong field and current. They applied this model to treat atom extraction in a Na/Vacuum/Na junction[11] and to study the current distribution and the barrier height between an aluminium tip and a silicon surface.[12]

In the present work, we study the influence of the electric field for different reasons: we wish to understand in which conditions the tip-induced electric field can influence the

STM contrast, and in particular why C_2H_4 molecules appear dark on the Si(001) surface. In order to understand such effects, we investigate the system in this paper using *ab initio* total energy and electronic structure calculations. A brief report on part of this work has already been submitted for publication.[13]

The paper is organized as follows. In Sec. II, the *ab initio* method we use is presented in more detail, and the geometry of the system is described. The results obtained for the bare Si(001) surfaces and for the adsorption of the ethylene molecule are described in Sec. III. Preliminary STM calculations are also presented in this section. In Sec. IV, we will see the necessity of including the effects of the tip-induced electric field on the surface wave functions in order to understand the STM contrast mentioned previously. The modifications to the total energy method implied by the presence of the electric field are also shown in this section. Sections IV B and IV C summarize the results obtained for the clean Si(001) surface and the surface on which ethylene molecules are deposited. STM images consistent with the experimental results are present in Sec. IV D. Finally we summarize the most significant results we have obtained (Sec. V). Additionally, in the appendix we clarify the relationship between the present calculations and the macroscopic electrostatics for a dielectric slab in periodic boundary conditions.

II. METHOD

In this study, we use the all-electron projector-augmented-wave (PAW) method recently developed by Blöchl.[14] This method goes beyond the pseudopotential method by using an augmented-plane-wave basis set which includes explicitly the difference between the true (all-electron) and pseudowave functions. The total all-electron wave function $|\Psi\rangle$ is taken to be equal to the smooth pseudowave function $|\tilde{\Psi}\rangle$ expanded in plane waves plus a one-center correction term

$$|\Psi\rangle = |\tilde{\Psi}\rangle + \sum_{i,R} (|\phi_i^R\rangle - |\tilde{\phi}_i^R\rangle)\langle \tilde{p}_i^R|\tilde{\Psi}\rangle. \quad (1)$$

The correction term is the sum of the difference between localized partial wave functions $|\phi_i^R\rangle$ (including the nodal structure of the full wave function, also called all-electron partial waves) and partial wave functions $|\tilde{\phi}_j^R\rangle$ corresponding to the nodeless pseudowave functions (pseudopartial waves). The sum is performed over atomic sites R and an index i representing the angular momentum values of the partial wave functions. Note that it is possible to have more than one partial wave function for the same angular momentum. The partial wave functions $|\phi_i^R\rangle$ and $|\tilde{\phi}_j^R\rangle$ are supposed to represent a complete expansion, within an augmentation sphere centered at the atomic site R, of the full $|\Psi\rangle$ and pseudowave $|\tilde{\Psi}\rangle$ functions respectively. The all-electron and pseudopartial waves coincide outside the augmentation region. Each individual term in the correction sum is weighted by the scalar product of the corresponding projector function $|\tilde{p}_i^R\rangle$ and the pseudowave function. The projector functions are constructed so as to be orthonormal (with respect to the indexes i and R) to the corresponding pseudopartial waves:

$$\langle \tilde{p}_i^R|\tilde{\phi}_j^{R'}\rangle = \delta_{ij}^{RR'}. \quad (2)$$

The use of local projectors permits one to obtain a generalized separable form for the nonlocal potentials.[15] This approach is similar in some ways to the separable non-norm-conserving pseudopotentials introduced by Vanderbilt,[16,17] but contains additional freedom for the atomic potential to adapt to the environment of the atom.

The calculations are carried out in the framework of the local density approximation[18] to density functional theory[19] using the Perdew and Zunger[20] parametrization of the exchange-correlation energy obtained by Ceperley and Alder.[21] We use two projectors for the silicon atom as well as for the carbon atom corresponding to s and p states (with an augmentation radius r_c of 0.50 a.u. for the silicon and 0.186 a.u. for the carbon) and one projector for the hydrogen atom (with an r_c of 0.186 a.u.). The method of calculating the projectors and partial wave functions is described in Sec. VI of Ref. 14. Note that all the projectors used in this work are norm conserving. Finally, the ground-state atomic and electronic configurations for the system are obtained via the Car-Parrinello method.[22] It should be noticed that, for such a method, the use of a separable form for the nonlocal potential is essential to reduce the computational effort.

The calculations are performed in a supercell ($14.51\times14.51\times41.04$ a.u.) containing 40 atoms (46 in the presence of adsorbed ethylene). We use the experimental cubic lattice constant of 5.43 Å. The 32 silicon atoms form an eight-layer slab with four atoms in each layer. Consequently the corresponding vacuum gap between the periodic images of the silicon slab is approximately 11.6 Å. This is large enough to include an adsorbed ethylene molecule on the surface without introducing significant interactions between slabs in the total energy calculations.

The bottom silicon layer is fixed to the corresponding bulk atomic positions and each Si dangling bond is saturated with a hydrogen atom. We are able to study those Si(001) reconstructions which are commensurate with our supercell; in the present case, these are the (2×1) symmetric and buckled (or asymmetric) dimers and the $p(2\times2)$ buckled dimer patterns. It is well known that other surface reconstructions, with larger periodicity, have been observed by STM.[2] However, we do not consider them in the present study because (i) the short-period reconstructions are supposed to be among the energetically most stable atomic configurations[23] and (ii) the interaction between the adsorbed molecule and the surface is very localized, so the long-range order in the reconstruction is not expected to be important.

In order to test the convergence of the calculations, we have used different values for the plane-wave cutoff energy ranging from 8 to 25 Ry and sampled the corresponding Brillouin zone with one or four k points [the Γ point or four k points from the irreducible part of the surface Brillouin zone: $k_\parallel=(0,0),(\pi/a,0),(0,\pi/b),(\pi/a,\pi/b)$], where a and b are the supercell sizes in the surface plane. The highest plane-wave cutoff energy (25 Ry) is more especially used for the calculations in the presence of the ethylene molecule. This value is needed to be able to describe well the short strong C-C bond in the molecule.

III. RESULTS

In this section we present the results we have obtained for the bare silicon surface and for the adsorption of ethylene

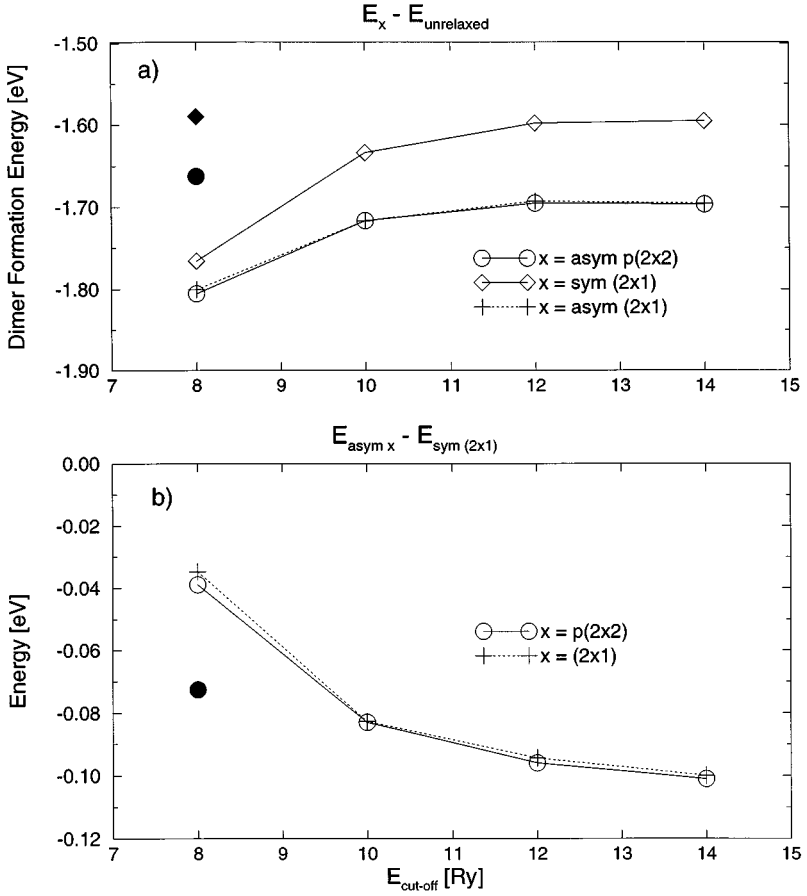

FIG. 1. (a) dimer formation energy (energy difference between the reconstructed and unreconstructed surface) and (b) ''buckling'' energy (energy difference between the asymmetric dimer and symmetric dimer configurations) versus the plane-wave energy cut off E_{cut}. The open symbols were obtained with the Γ point only, and the filled symbols with four k points parallel to the surface.

molecules on the Si(001) surface. Finally from the electronic structure of the relaxed C_2H_4-Si(001) system, we derive a STM calculation in order to understand the experimental observations.

A. The bare Si(001) surface

Our purpose is neither to perform a complete and detailed analysis of all the possible Si(001) surface reconstructions, nor to settle the controversy about the relative stability of all the different Si(001) dimer configurations. We consider only three different dimer configurations: the (2×1) symmetric and asymmetric dimers and the $p(2\times2)$ asymmetric dimers. The two latter asymmetric configurations are the most commonly observed by STM even though the $c(4\times2)$ configuration has been also observed.[2] However it has been recognized that the $c(4\times2)$ and $p(2\times2)$ are almost degenerate.[23]

First we determine the fully relaxed electronic and atomic structures for the three different dimer configurations using the plane wave cutoff energy $E_{\mathrm{cut}}=8$ Ry and Γ-point sampling. The relaxation of both the electronic and atomic degrees of freedom is obtained by introducing a damping factor in the Car-Parrinello equations of motion. The relaxation is stopped when all components of all the forces on the atoms are smaller than 5×10^{-4} Hartree/Bohr ($\approx$26 meV/Å). Using the resulting slab geometry, calculations are performed for higher E_{cut} values and improved k-point sampling. The results for the dimer formation energy as well as for the energy difference between asymmetric and symmetric dimers are shown on Fig. 1. The asymmetric (2×1) and $p(2\times2)$ dimers are energetically more stable than the symmetric (2×1) dimer, with slightly smaller total energy values for the $p(2\times2)$ configuration. These results are in good agreement with others in the literature.[23,24] We have verified that the atomic relaxation is not crucial for the energy values shown on Fig. 1. For example, a full relaxation of the symmetric (2×1) structure, obtained for $E_{\mathrm{cut}}=12$ Ry and the same criterion on the final force values as previously, lowers the total energy only by a small amount ($\approx$3.5 meV/dimer) which is close to the limit of resolution of the present method. Furthermore the asymptotic limit of the energy difference between the asymmetric and symmetric dimers (≈-0.10 eV/dimer) is the same as that obtained by Dabrowski and Scheffler.[24] The final dimer bond lengths we obtained are respectively 2.21, 2.23, and 2.24 Å for the symmetric (2×1), asymmetric (2×1), and $p(2\times2)$ dimers, about midway between the single and double Si-Si bond lengths. The values for the buckling angles are 12° and $\pm16°$ for the asymmetric (2×1) and $p(2\times2)$ configurations. These values are in qualitative agreement with the literature but slightly different from those obtained by Dabrowski and Scheffler.

B. Adsorption of ethylene molecules on the Si(001) (2×1) surface

The detailed calculations of the adsorption of the ethylene molecules on the Si(001) surface have been already described elsewhere.[25] Let us recall the main results that have been obtained. The authors consider the Si(001) surface with

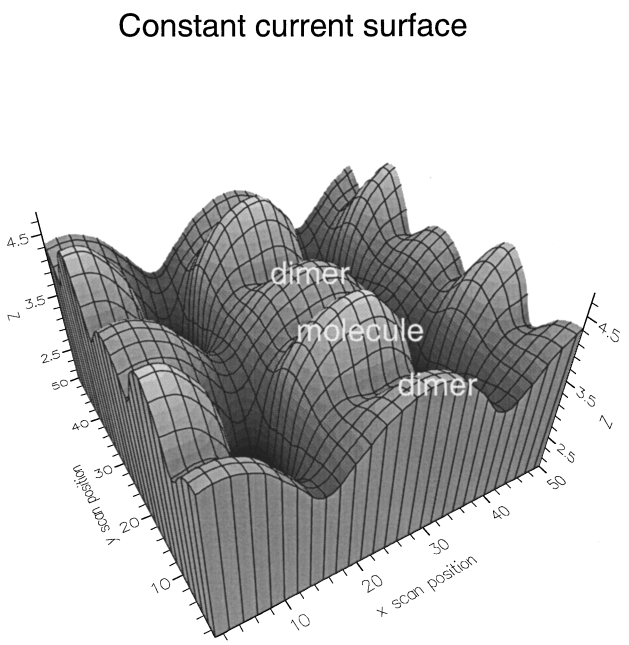

FIG. 2. Constant current $\overline{j}$ scans above the surface unit cell obtained for zero electric field. The normalized $\overline{\sigma_{\mathrm{av}}}/(2e^2/h)$ value is 1×10^{-4}. $V=(\mu_i-\mu_f)/e\approx0.9$ V. The ''tip-sample'' distance Z is given in Å and corresponds to the position of the center of the Gaussian final state. For the definition of this distance see text (Sec. IV C). Note that for $Z=0$ ($Z\approx2.4$ Å) the final state is located at the same height as the upper atom of the clean dimer (as the hydrogen atoms of the ethylene molecule). The image shows that the molecules appear brighter than the bare dimers.

an asymmetric $p(2\times2)$ dimers reconstruction and one C_2H_4 molecule in the unit cell which corresponds to a coverage rate of 50%. The fully relaxed calculations performed for $E_{\mathrm{cut}}=25$ Ry and the Γ-point sampling show that the ethylene molecule adsorbs on top of the dimer. This situation corresponds to the minimum total energy configuration where the C-C bond of the molecule lies parallel to the Si-Si dimer bond underneath as shown on Fig. 2 of Ref. 13. In this case, the hybridization of the carbon atoms changes from sp^2 (free ethylene molecule) to sp^3 with a corresponding increase of the C-C bond length from 1.33 to 1.53 Å. Another important point is that even although the dimer beneath the adsorbate is almost flat (buckling angle of $\approx1°$) and the dimer bond length is larger (2.286 Å) than the Si-Si bulk bond length, the dimer bond *remains intact*. The other dimer in the unit cell is only slightly affected by the presence of the adsorbate. It is still tilted (buckling angle of 9.6°) and the dimer bond length is slightly increased (2.248 Å) as compared to the corresponding value in absence of the adsorbate. Finally the calculated adsorption energy for a single ethylene molecule (1.57 eV) is in agreement with values deduced from thermal desorption measurements (1.65 ± 0.07 eV).[26]

C. STM imaging

In order to understand the origin of the contrast observed in STM images of the ethylene molecules adsorbed on the Si(001) surface, STM calculations have been performed. For this, we use a nonperturbative method for calculating the tunneling current.[27] This method goes beyond the Tersoff-Hamann approximation[5] and can be used with the self-consistent potential and wave functions obtained from *ab initio* calculations. In this model, the measure of the tip-sample tunneling current is taken as the time-averaged rate of electron transfer between two electronic states, localized on either side of the tunneling junction. In principle, this method can be related to scattering approaches for the tunneling current developed by other authors if the initial and final states are correct asymptotic scattering states. Given that an electron is initially in the state $|i\rangle$, the time-averaged tunneling current into a final state $|f\rangle$ is expressed as[27]

$$\overline{j}=2e\frac{\eta^2}{h}\int_{\mu_f}^{\mu_i}dE|\widetilde{G}_{fi}(E+i\eta)|^2, \tag{3}$$

where μ_i and μ_f are the electrochemical potentials of the initial and final states respectively, $\eta=\hbar/2\tau$ (τ being the averaging time) and $\widetilde{G}_{fi}$ is the Green's function matrix element connecting the initial state to the final state. For a given energy the corresponding time-averaged differential conductance may be written as

$$\overline{\sigma(E)}=\frac{2e^2}{h}\eta^2|\widetilde{G}_{fi}(E+\mathrm{i}\eta)|^2. \tag{4}$$

The factor of 2 arises from the electron spin. The advantage of the method is that the Green's function can be determined from the (Kohn-Sham[18]) single-particle eigenstates $|n\rangle$ of the system whose eigenvalues are E_n. Therefore the Green's function matrix element $\widetilde{G}_{fi}$ is expressed as usual by

$$\widetilde{G}_{fi}(E)=\sum_n\frac{\langle f|n\rangle\langle n|i\rangle}{E-E_n}. \tag{5}$$

In principle, the $|n\rangle$ are the eigenstates of the supercell containing the surface slab, the adsorbed molecule and the tip. However, as a first step of calculation and in order to reduce the computational time, we introduce some approximations. First we consider only the eigenstates of the supercell containing the surface slab and the adsorbed molecule. However, note that a part of the tip potential will be included in some of our calculations (see Sec. IV D). The differential conductance is calculated for a set of N_E different energies E_α relevant for the experiments, i.e., close to the top of the valence band. Then these conductance values are summed over the corresponding energy window $\Delta E=\mu_i-\mu_f=$ eV to give an approximation of the integral in Eq. (3): $\overline{j}=V\overline{\sigma}_{\mathrm{av}}=V\Sigma_\alpha\overline{\sigma(E_\alpha)}/N_E$. Finally, inherent to the model, the use of localized states $|i\rangle$ and $|f\rangle$ is essential to obtain an expression for the tunnel current that can be used in a supercell calculation (i.e., a system with periodic boundary conditions). However, such states do not describe the asymptotic scattering states obtained when the tunneling is viewed as a scattering process.[28,29] In order to check that our choice of localized states does not bias the results, we perform an incoherent summation of the differential conductance over a set of randomly localized Gaussian initial states in the substrate. The final state $|f\rangle$ is chosen to be a localized Gaussian in the vacuum region; this state moves through space as the tip scans. The details of the method of calculation for such a conductance, as well as an analysis of the limits and the extension of the method, will be presented elsewhere.

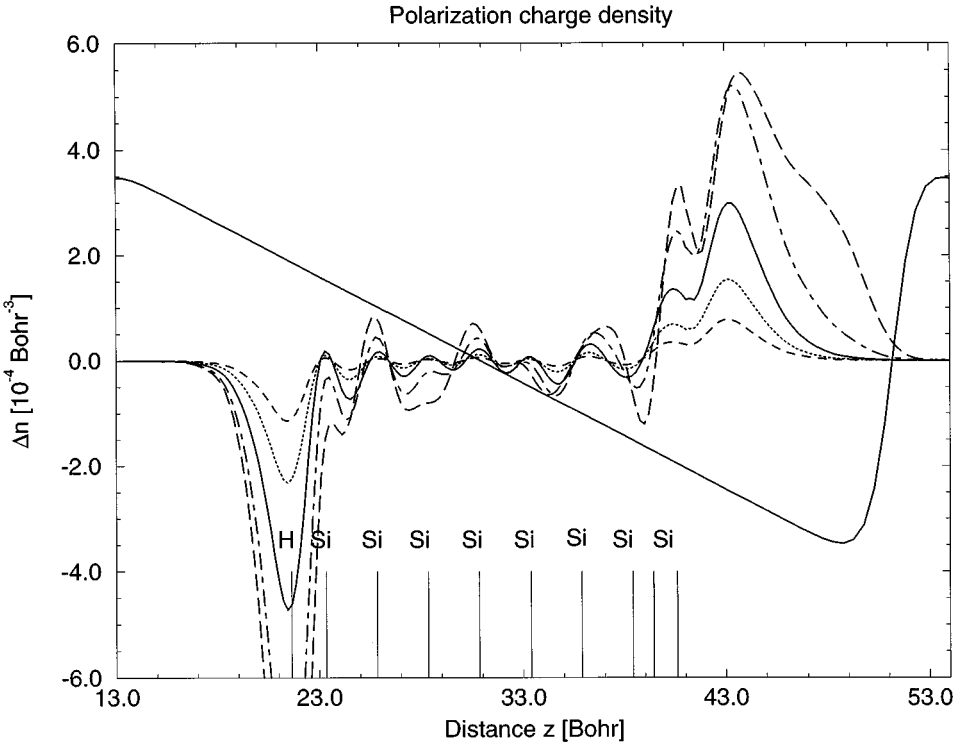

FIG. 3. Average over the (xy) plane (parallel to the surface) of the polarization charge density $\Delta\tilde{n}$ versus the z coordinate for the clean Si(001) $p(2\times2)$ surface. $\Delta\tilde{n}(z)$ is shown for different values of the tip-induced electric field ξ^{ext}: (a) -0.002 a.u. (0.10 V/Å) dashed line, (b) -0.004 a.u. (0.21 V/Å) dotted line, (c) -0.008 a.u. (0.41 V/Å) solid line, (d) -0.015 a.u. (0.77 V/Å) dot-dashed line, (e) -0.020 a.u. (1.03 V/Å) long-dashed line. The z dependence of V^{ext} is also represented by a solid line (reduced amplitude). The solid vertical lines mark the positions of the different slab layers (the extreme left one is for the hydrogen layer and the two extreme right ones are respectively for the lower and upper Si atoms of the dimer).

An example of an STM image obtained from this method for the C_2H_4 deposited on the Si(001) surface is shown on Fig. 2. These calculations reveal that, for the chosen constant current value, the ethylene molecules appear higher than the bare dimers themselves. Constant-current j scans over the molecule and the bare dimer have also been performed for different values of the conductance (see Fig. 3 in Ref. 13). It has been shown that the molecules always appear higher than the bare dimers which is in contradiction with the experimental results.

We have also verified that the electronic density of the highest occupied states (eigenstates whose energies are included inside the energy window ΔE for which the conductance has been calculated) is always larger above the molecules than above the bare dimers (for any reasonable values of the z coordinate above the surface). Thus, images calculated within the perturbative Tersoff-Hamann approximation also show the molecules as higher than the dimers. In such conditions, we are not able to interpret the observed contrast in STM images. How, then, can we understand the experiments?

IV. PRESENCE OF AN EXTERNAL ELECTRIC FIELD

It is well known that the presence of the tip close to the surface can play an important role for the understanding of STM images. When the tip is very close to the surface, strong modifications of both the tip and sample electronic structure and even of their atomic structure can occur. However, according to the experimental observations, such strong modifications have not been reported in this system. Another effect arising from the presence of the tip is due to the difference of potential existing between the tip and the sample. This implies the existence of an electric field inside the tunneling junction. For typical bias values (1–3 V) and estimated tip-sample separations (3–6 Å), the values of the corresponding electric field vary between 0.16 and 1.00 V/Å.

This tip-induced electric field will polarize the surface. Furthermore the value of the dielectric constant of silicon[30] ($\epsilon_r=12.0$) is larger than those of organic (alkane like) systems; for example, $\epsilon_r=1.70$ for methane, while ϵ_r varies from 1.33 to 1.87 for propene and from 1.90 to 2.00 for hexane as the temperature varies.[31] Consequently we expect that the silicon surface is more polarizable than the adsorbed molecules. This suggests that when an electric field is directed towards the surface (corresponding to the situation of tunneling out of the surface), the electrons are ''pulled out'' into the tunneling barrier in a different way for the surface and the molecules. Starting from this qualitative idea we now investigate quantitatively the effects of an electric field on the Si(001) surface with and without deposited ethylene molecules. The method we use and the results obtained are described in the remainder of this section.

A. Method

In order to study the influence of the tip-induced electric field on both the electronic and atomic structures of Si(001)

surfaces, we add into the calculations an external electric field. As a first step of approximation, we consider a uniform electric field lying in the direction perpendicular to the surface. Such an approximation implies that the tip's radius of curvature is large relative to the size of the surface cell, which is not unreasonable. It should be remembered that the electrostatic forces extend over much longer distances than the tunneling process.

The corresponding linearly varying external potential must be made commensurate with the periodic supercell in the direction perpendicular to the surface (which we take as the z direction in what follows). The procedure we adopt is equivalent to adding a double layer of charges in the vacuum gap between the slab. The external potential is written as

$$V^{\text{ext}}(z)=\xi^{\text{ext}}[z-z_0-a_3 f(z-z_c)] \quad \text{for } 0\leqslant z\leqslant a_3, \tag{6}$$

where ξ^{ext} is the value of the electric field, z_0 is the position of the zero of the external potential and a_3 is the length of the supercell along the surface normal. The function $f(z)$ introduces a discontinuity in the linear potential; this is necessary so that the potential becomes periodic, as required for periodic supercell calculations. In their work concerning atomic desorption in high electric fields, Neugebauer and Scheffler used for $f(z)$ the heavyside-step function.[9] However, such a discontinuous function is not accurately described by a finite Fourier series necessary to perform the calculations in reciprocal space. Hence, we have introduced a smoother function. A natural way for choosing this function is to use the same mathematical form as for the Fermi-Dirac distribution,

$$f(z-z_c)=\frac{1}{1+e^{\beta(z_c-z)}}. \tag{7}$$

The parameter β permits us to adjust the smoothness of the function and z_c is the position of the discontinuity in the case of an infinite value for β. In practice we choose z_0 in the middle of the slab and z_c in the middle of the vacuum gap. Since the function $f(z)$ is almost equal to zero when $\beta(z_c-z)\gg 1$, we have a uniform electric field over the region of the sample slab: $V^{\text{ext}}(z)\approx\xi^{\text{ext}}(z-z_0)$.

The presence of the external potential introduces additional terms in the expression for the total energy of the system,

$$\Delta E^{\text{ext}}=\int n(\mathbf{r})V^{\text{ext}}(\mathbf{r})d\mathbf{r}-\sum_I Z_I V^{\text{ext}}(\mathbf{R}_I). \tag{8}$$

ΔE^{ext} is the interaction energy of the external potential V^{ext} with the all-electron charge density $n(\mathbf{r})$ and with the point charges Z_I (atomic number or charge of the nucleus of the Ith atom located at $\mathbf{R}_I$).

In the PAW method, the all-electron charge density is decomposed into three contributions,

$$n(\mathbf{r})=\tilde{n}(\mathbf{r})+n^1(\mathbf{r})-\tilde{n}^1(\mathbf{r}). \tag{9}$$

$\tilde{n},n^1,\tilde{n}^1$ are the charge densities associated with the pseudowave functions $|\tilde{\Psi}\rangle$ (plane waves), the all-electron partial waves $|\phi_i^{R_I}\rangle$, and the pseudopartial waves $|\tilde{\phi}_i^{R_I}\rangle$, respectively [cf. Eqs. (14)–(17) of Ref. 14]. The partial waves are expressed as the product of radial functions with spherical harmonics. Note that each charge density contains the contribution of its respective core states. The interaction energies of V^{ext} with the different parts of the charge density are calculated in different ways. The interaction with $\tilde{n}$ is calculated in reciprocal space as in standard plane-wave calculations (in real space for the associated core charge density $\tilde{n}^c$). The interaction with the one-center densities $n^1,\tilde{n}^1$ is obtained from the spherical-harmonic representation of V^{ext} around each atomic site $\mathbf{R}_I$,

$$V^{\text{ext}}(\mathbf{r}-\mathbf{R}_I)=\sqrt{4\pi}\xi^{\text{ext}}(z_I-z_0)Y_{0,0}+\sqrt{4\pi/3}\xi^{\text{ext}}|\mathbf{r}-\mathbf{R}_I|Y_{1,0}(\theta,\varphi). \tag{10}$$

The generalization for any direction of the electric field is straightforward and includes terms with $Y_{1,\pm 1}$. This representation of V^{ext} is reminiscent of the expression of the partial wave functions $|\phi\rangle$ and $|\tilde{\phi}\rangle$ from which the one-center densities are constructed. A similar decomposition for an ''external'' field can be found in Ref. 32.

Similarly, additional terms for the forces on the atoms must be included. The components of the force on a particular atom labeled I are obtained from the following standard expression:

$$F_{I,(x,y,z)}=-\frac{\partial\Delta E^{\text{ext}}}{\partial R_{I,(x,y,z)}}=-\nabla_{I,(x,y,z)}\Delta E^{\text{ext}}. \tag{11}$$

According to the symmetry of the present electric field, only the z component of these additional forces is nonvanishing. However, it can be seen that a generalization to any direction of the electric field is also straightforward. We will see that the additional forces can be expressed in three different contributions. The first one, easy to derive, comes from the second term in the right-hand side of Eq. (8). It corresponds to the force exerted by a uniform electric field on a point charge,

$$F_{I,z}^{(1)}=Z_I\xi^{\text{ext}}. \tag{12}$$

Following the same procedure to determine the forces for the PAW method as in the original paper,[14] we obtain the other terms. Since the pseudocharge density $\tilde{n}$ contains implicity the corresponding pseudocore charge density $\tilde{n}^c$, there exists a force acting on this charge density,

$$F_{I,z}^{(2)}=-\nabla_{I,z}\int\tilde{n}(\mathbf{r})V^{\text{ext}}(\mathbf{r})d\mathbf{r}. \tag{13}$$

It can be shown after a little algebra that this term reduces to a simpler expression $F_{I,z}^{(2)}=-\tilde{N}_I^c\xi^{\text{ext}}$, where $\tilde{N}_I^c=\int\tilde{n}^c(\mathbf{r}-\mathbf{R}_I)d\mathbf{r}$ is the charge of the pseudocore of the Ith atom. No assumption on the electric field inside the core region has been used, even if the previous result seems to imply that the field is constant over the core region. This result can be understood by the fact that (i) the spherical-harmonic expansion of $\tilde{n}^c$ includes only a purely spherical s component (this is a convenient choice since by construction $\tilde{n}^c$ is arbitrary to some extent) and (ii) $\tilde{n}^c$ is short ranged and does not overlap with the ''fictitious'' double layer of charges associated with V^{ext}. $F_{I,z}^{(1)}$ and $F_{I,z}^{(2)}$ can be summed to give an effective force on the total core charge associated to the Ith atom $F_{I,z}=(Z_I-\tilde{N}_I^c)\xi^{\text{ext}}$. This is the standard expression for the

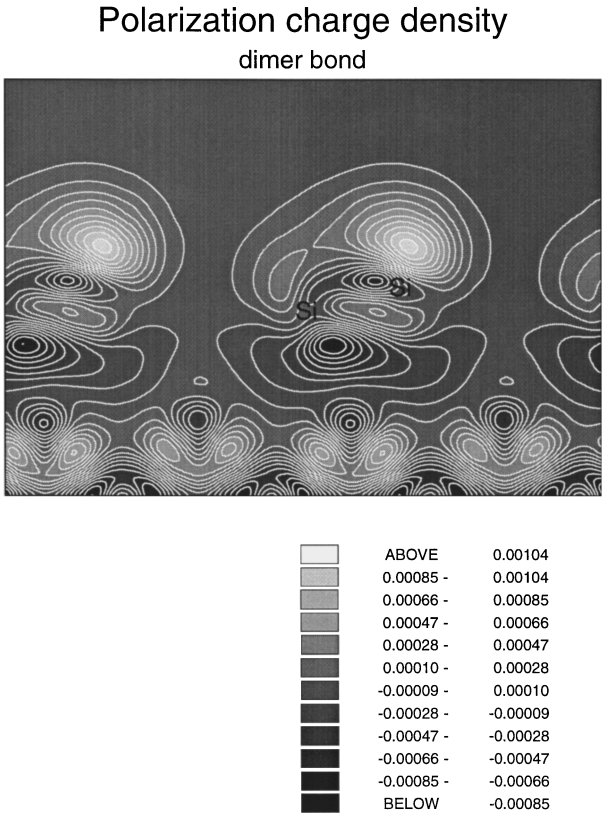

FIG. 4. Polarization charge density $\Delta\tilde{n}$ in the $(1\bar{1}0)$ plane along the dimer Si-Si bond. The values of the charge density contours are given in [electron/Bohr^3] as in the following figures. Accumulation of charge can be seen above the upper dimer atom and charge depletion below the Si-Si bonds. The value of the electric field is $\xi^{\text{ext}}=-0.008$ a.u. (0.41 V/Å). The dimer Si atomic positions are also indicated.

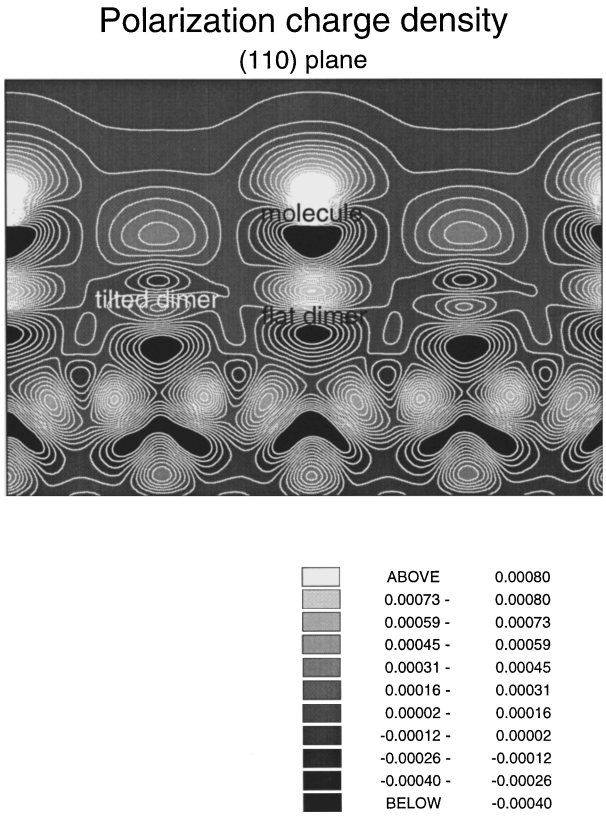

FIG. 5. Polarization charge density $\Delta\tilde{n}$ in the (110) plane passing through the middle of the dimer Si-Si bond and the C-C bond of the molecule. The successive accumulation and depletion of charge (form the top to the bottom) are attributed to the polarization of the C-C and Si-Si bonds, respectively. Here $\xi^{\text{ext}}=-0.008$ a.u. (0.41 V/Å).

forces on the atomic core derived from pseudopotential plane-wave calculation. The last term comes from the one-center densities n^1 and $\tilde{n}^1$

$$F_{I,z}^{(3)}=-\nabla_{I,z}\int [n^1(\mathbf{r})-\tilde{n}^1(\mathbf{r})]V^{\text{ext}}(\mathbf{r})d\mathbf{r}. \tag{14}$$

This force is due to the change of shape of the one-center densities as the atoms move and is derived in the same manner as Eqs. (51)–(57) of Ref. 14. The force $F_{I,z}^{(3)}$ is expressed as

$$F_{I,z}^{(3)}=-\sum_{ij}\nabla_{I,z}\Theta_{ij}^{R_IR_I}(\langle\phi_i^{R_I}|V^{\text{ext}}|\phi_j^{R_I}\rangle-\langle\tilde{\phi}_i^{R_I}|V^{\text{ext}}|\tilde{\phi}_j^{R_I}\rangle). \tag{15}$$

Since $V^{\text{ext}}(\mathbf{r})$ is a local potential, it acts on the same atomic site $\mathbf{R}_I$ for the all-electron partial wave $|\phi_i^{R_I}\rangle$ and pseudopartial wave $|\tilde{\phi}_i^{R_I}\rangle$. Let us recall that the indexes i and j represent the angular momentum (l,m) of the corresponding partial wave and other additional indices, if used, to label different partial waves for the same angular momentum. $\Theta_{ij}^{RR'}$ is a density matrix for the one center expansion in terms of partial waves and is defined as

$$\Theta_{ij}^{RR'}=\sum_n f_n\langle\tilde{\Psi}_n|\tilde{p}_i^R\rangle\langle\tilde{p}_j^{R'}|\tilde{\Psi}_n\rangle, \tag{16}$$

where $|\tilde{\Psi}_n\rangle$ is the pseudowave function with occupation f_n and $|\tilde{p}_i^R\rangle$ is the projector function of angular momentum (l,m) located at the atomic site R. In the context of the PAW method, the force $F_{I,z}^{(3)}$ is reminiscent of Pulay-like forces.[33] We refer to the original PAW paper for readers who are interested in the practical way such forces are calculated. Including the different expressions we have derived for the additional terms in the total energy and forces on the ions, we can calculate the self-consistent electronic charge density as well as the ground-state atomic positions in the presence of the external potential V^{ext}.

B. Effects of the electric field on the bare Si(001) surface

We apply the results described in the previous section to the Si(001) $p(2\times2)$ surface. First we study the influence of the external electric field on the electronic structure of this surface. The atomic geometry for the slab is the same as that obtained in Sec. III A. The calculations are performed for $E_{\text{cut}}=8$ Ry and Γ-point sampling. The field is directed towards the surface as in a STM experiment for which the electrons tunnel out of the surface. Different values of ξ^{ext}

have been used. They are typical for standard STM experiments and range from 8×10^{-3} to 15×10^{-3} a.u. (0.10 to 0.77 V/Å).

We define the polarization charge density Δn by

$$\Delta n(\mathbf{r}) = n(\mathbf{r}, \xi^{\text{ext}}) - n(\mathbf{r}, \xi^{\text{ext}}=0). \tag{17}$$

However, we are mostly interested in the behavior of the charge density outside the surface. Therefore, owing to the localization of the partial waves in the augmentation region around each atom, the variation under the electric field of the all-electron charge density in the vacuum is essentially given by the total pseudocharge density $\tilde{n}$. Furthermore, in general, the polarization of the one center densities is smaller than the polarization charge density $\Delta\tilde{n}$. Figure 3 represents the variation of the polarization charge density $\Delta\tilde{n}$ [averaged over the (xy) plane parallel to the surface] with respect to the z coordinate. The main changes occur at the surfaces of the slab. As expected and according to the sign of the electric field, we find an increase of the electron density at the surface and in the vacuum (and a corresponding decrease on the other side of the slab). The charge accumulation and depletion at the slab surfaces can be related to a surface charge density and the corresponding classical polarization vector using standard electrostatics as we show in the appendix. The amplitude of the accumulation charge density peak increases with increasing electric field. However, the position of the maximum of this peak is not strongly modified except for the highest value of ξ^{ext} shown in Fig. 3. For this and higher values of the electric field another phenomenon occurs. The strong modification of the accumulation charge peak corresponds to states which are trapped in the artificial potential well created by the cutoff function $f(z)$ defined in Sec. IV A. In the following, we always check that there are not unphysical ''trapped'' states for the electric field values we use. Inside the slab, oscillations of the polarization charge density can be seen. They have a small amplitude and do not strongly depend on the value of the electric field (at least for the range we have considered).

In order to illustrate the modifications of the charge density above the dimers, Fig. 4 represents the polarization charge density $\Delta\tilde{n}$ in the (110) plane containing the dimer bond. There is a strong increase of the charge density above the upper dimer atom and decrease of the charge density below the dimer bond (almost located below the lower dimer atom). Such a qualitative behavior has already been observed by Huang *et al.*[10] However, note that in their calculation, these authors did not take into account the atomic relaxation due to the presence of the electric field. This polarization charge density plot (Fig. 4 and part of Fig. 5) is characteristic of the complex polarization both of the Si-Si dimer σ bond and of the π dangling bonds, and also of the polarization of the bonds between the dimers and the remainder of the surface.

Finally we have performed a full (electronic and atomic) relaxation calculation for the Si(001) $p(2\times2)$ surface in the presence of the field. The initial slab geometry is the same as previously. Since we are mostly interested in the modifications of the atomic structure of the surface, the atomic positions of the hydrogen layer and of the two silicon bottom layers were fixed. Calculations were performed again for

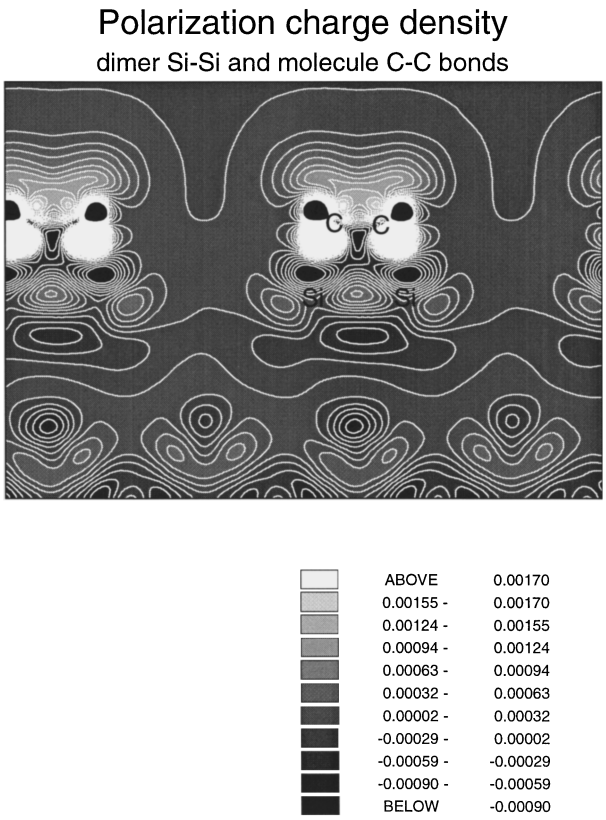

FIG. 6. Polarization charge density $\Delta\tilde{n}$ in the $(\bar{1}10)$ plane containing the dimer Si-Si and molecule C-C bonds for $\xi^{\text{ext}}=-0.008$ a.u. (0.41 V/Å). The polarization of the different bonds (C-C, Si-C, and C-H) can be seen (see text).

$E_{\text{cut}}=8$ Ry and the Γ-point sampling. The atomic positions were relaxed until the forces on all the atoms are smaller than 7×10^{-4} Hartree/Bohr (≈36 meV/Å).

The main modifications due to the presence of the electric field are observed on the dimer atoms; the other atoms inside the slab are not displaced (their displacements are less than 0.05 Å). The upper dimer atom is slightly displaced towards the vacuum whereas the lower atom moves towards the slab by an amount of approximately 0.16 Å. Consequently we observe an increase of both the dimer bong length (2.256 Å) and the buckling angle (19.7°) as compared to the values in the absence of the electric field. Such a modification of the buckling angle under an electric field has also been obtained in a semiempirical calculation by Ramos *et al.*[34] This behavior is consistent with the standard picture of charge transfer from the partially occupied dangling bond on the lower dimer atom to that of the upper atom. This leads to a positively (negatively) charged lower (upper) dimer atom.[34,35] Thus given the direction of the electric field, the charged atoms move as we expect. The values we have given for the bond length and the buckling angle are obtained for $\xi^{\text{ext}}=8\times10^{-3}$ a.u. (≈0.41 V/Å). These values are lower (larger) for a lower (larger) amplitude of the electric field. Finally note that the atomic displacements induced by the electric field we obtain are larger than those calculated by Huang *et al.*[10] This may be in part because they estimate the response of the surface to an applied force by displacing the

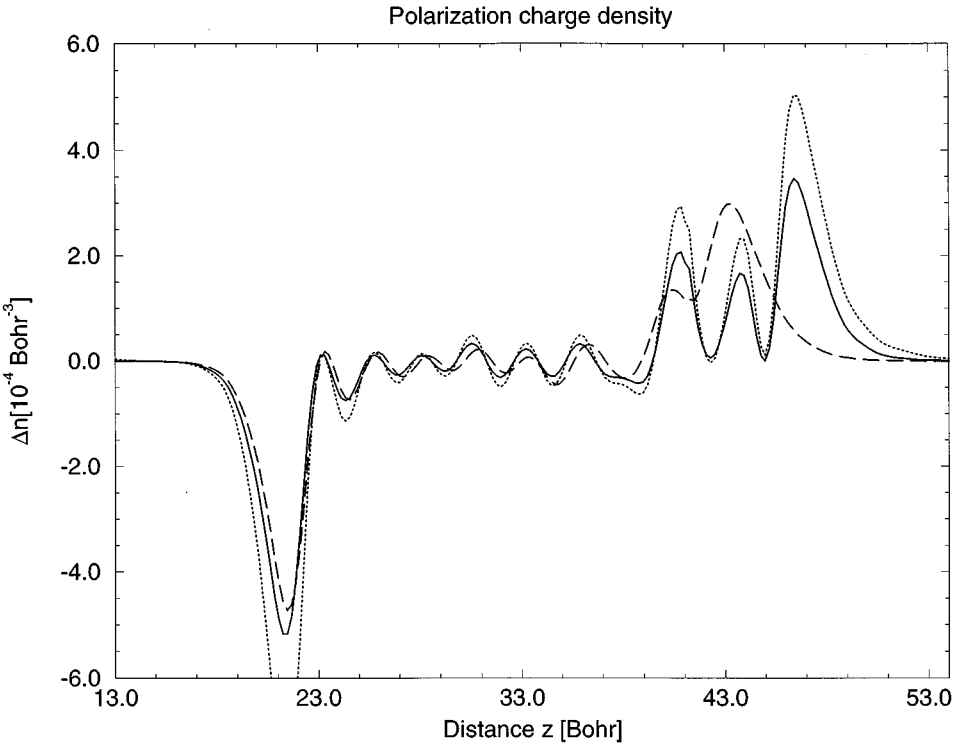

FIG. 7. (xy)-averaged polarization charge density $\Delta\tilde{n}$ versus the z coordinate for the Si(001) surface on which ethylene molecules are adsorbed. The values of the electric field are ξ^{ext} (i) -0.008 a.u. (0.41 V/Å) solid line, (ii) -0.012 a.u. (0.62 V/Å) dotted line. Compare the rate of decay of $\Delta\tilde{n}$ in the vacuum to the corresponding decaying polarization charge density of the clean Si(001) (long-dashed line, $\xi^{\text{ext}}=-0.008$ a.u.).

dimer alone with no additional relaxation. This procedure would be expected to overestimate the stiffness of the surface.

Finally, it should be noticed that the effects of the applied electric field presented here are purely localized at the surface (at the atomic scale relevant for tunneling imaging). For a realistic semi-infinite surface other effects also occur, such as long-range band bending below the surface. The corresponding depletion lengths or screening lengths are, however, very large compared with the size of our system (typically of the order of hundreds of Å, depending on the dopant concentration and surface defects in the system). Therefore such a screening has a negligible effect on the properties of the surface at an atomic scale. However, the screening and associated band bending will strongly influence the relationship between the total bias applied to the STM and the voltage actually appearing across the tunneling junction. This point, crucial for scanning tunneling spectroscopy, has been investigated recently by several different authors (see for example Refs. 36 and 37). In any case there are also further uncertainties in the tip-induced field arising from the unknown tip shape and tip-sample separation.

C. Effects of the electric field on the C_2H_4-Si(001) system

We now investigate the effects of the electric field on the Si(001) surface on which ethylene molecules are adsorbed. We use the same atomic geometry for the slab as obtained in the absence of the electric field and for $E_{\text{cut}}=25$ Ry (Γ point), cf. Sec. III B. The electronic wave functions are relaxed in the presence of the field. The polarization charge density along the plane passing through the bare dimer and the plane containing the other dimer and the C-C bond of the adsorbate has been determined. The same trends described above remain for the bare dimer. However, a more complicated feature appears on and near the adsorbed molecule. For example, the polarization charge density in the (110) plane passing through the middle of the Si-Si and C-C bonds is shown in Fig. 5. A succession of positive and negative values of $\Delta\tilde{n}$ is obtained. According to the atomic positions, each pair of high and low density values corresponds to the polarization of a bond (the Si-Si and C-C bond respectively). In the (110) plane containing the dimer and C-C bonds, the polarization charge density shows even more structure (Fig. 6). The accumulation and depletion of charge in the region between the dimer and C-C bonds are attributed to the polarization of the Si-C bonds themselves. The strong depletion of electronic charge located on each side of the carbon atoms is mainly due to the polarization of the C-H bonds. Finally the lobe of charge accumulation above the molecule originates essentially from the polarization of the carbon and hydrogen atoms themselves.

The xy-averaged polarization charges densities obtained for different values of ξ^{ext} are shown on Fig. 7. An accumulation of charge, outside the surface, is clearly seen. The polarization charges density decays exponentially in the vacuum gap as expected. However, one can see that the slope of the decaying charge density is different for the bare surface as compared to the one for the surface supporting ad-

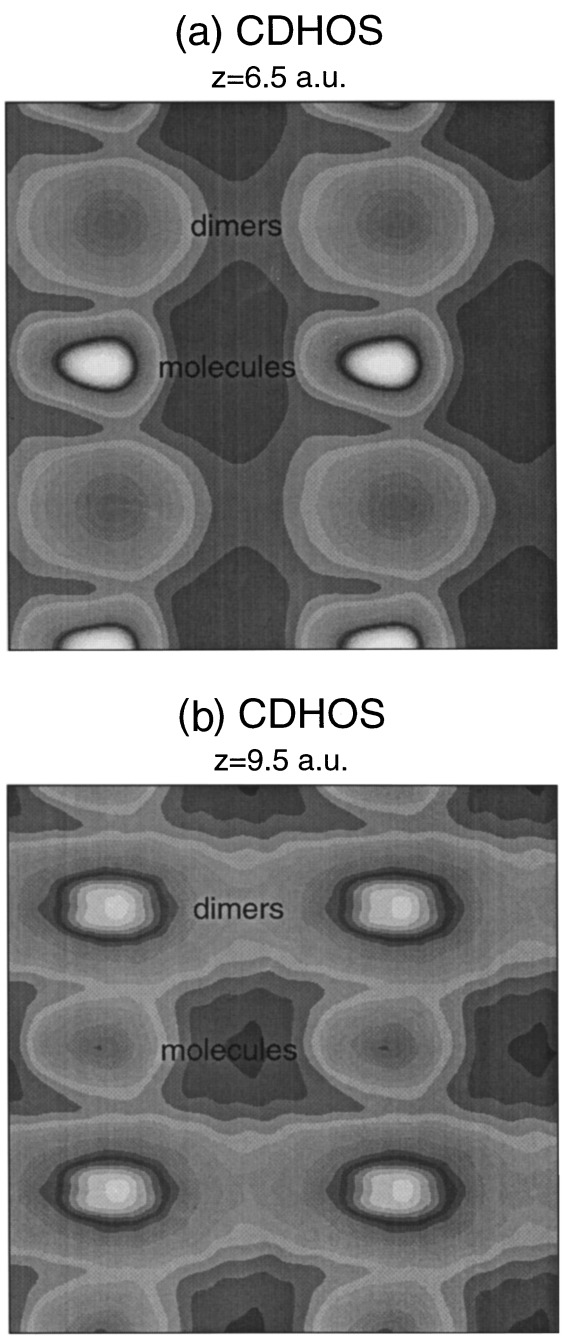

FIG. 8. Charge density of the highest occupied states (CDHOS) in a plane parallel to the surface ($\xi^{\mathrm{ext}}=-0.008$ a.u.). The planes are located in the vacuum at (a) $z=6.5$ a.u., the molecules appear brighter than the dimers, and (b) $z=9.5$ a.u, an inversion of the contrast in the CDHOS plots is observed.

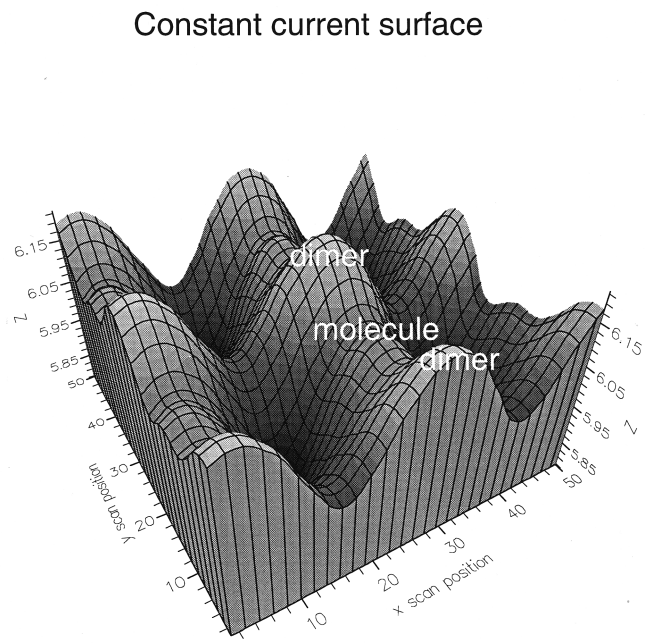

FIG. 9. Constant current $\overline{j}$ scans above the surface unit cell obtained for an applied electric field $\xi^{\mathrm{ext}}=-0.008$ a.u. (-0.41 V/Å). The normalized $\overline{\sigma_{\mathrm{av}}}/(2e^2/h)$ value is 1×10^{-4} and $V=(\mu_i-\mu_f)/e\approx0.9$ V. The ''tip-sample'' distance Z is given in Å. The contrast is inverted as compared to Fig. 2 and the molecules appear sightly darker than the clean silicon dimer in agreement with the experimental results.

sorbates. This suggests that there is a different behavior of the decaying charge density above the adsorbed molecule and the bare dimer.

In order to clarify this point and to shed some light on the STM contrast observed on the adsorbates, we have calculate the charge density of the highest occupied states (CDHOS) in planes parallel to the surface. The CDHOS is obtained from the surface states whose energy lies, at the top of the valence band, in the energy window taken to integrate the tunneling current Eq. (3). The CDHOS has been calculated for two different values of the z coordinate ($z=6.5$ and 9.5 a.u.). This corresponds to planes located in the vacuum at a distance of approximately 3.6 and 5.2 Å respectively from the bare Si(001) surface (or 1.2 and 2.8 Å respectively from the top of the C_2H_4 molecule). The CDHOS in these planes are represented on Fig. 8. For the lowest z value, the density is higher above the molecule than above the bare dimer. For the distance further away from the surface ($z=9.5$ a.u.) we observe the opposite. Obviously there is a turning point z_{tp} above which the density on top of the bare dimer is larger than above the adsorbed molecule. In other words, the CDHOS above the ethylene molecule decays faster in the vacuum than the density above the dimer. In order to use these results for understanding the contrast in STM images, we first use the simple Tersoff-Hamann picture for obtaining the tunneling current. It consists of taking the tunneling current simply proportional to the surface electronic density at energies close to the Fermi level[5] (e.g., I_{tunnel} is proportional to the CDHOS). We choose a constant current value for which the corresponding tip-sample distance is always larger than z_{tp}. Then it is easy to show from Fig. 8 that in the corresponding constant CDHOS surface, the C_2H_4 molecule appears slightly darker than the bare dimer as observed experimentally. (Note that this simple picture for STM imaging does not correspond exactly to the original Tersoff-Hamann approximation since we have considered the surface electronic structure modified by the presence of the tip-induced electric field.) However, for the moment this interpretation is only based on surface electronic density considerations. Therefore in order to test the accuracy of such an approxi-

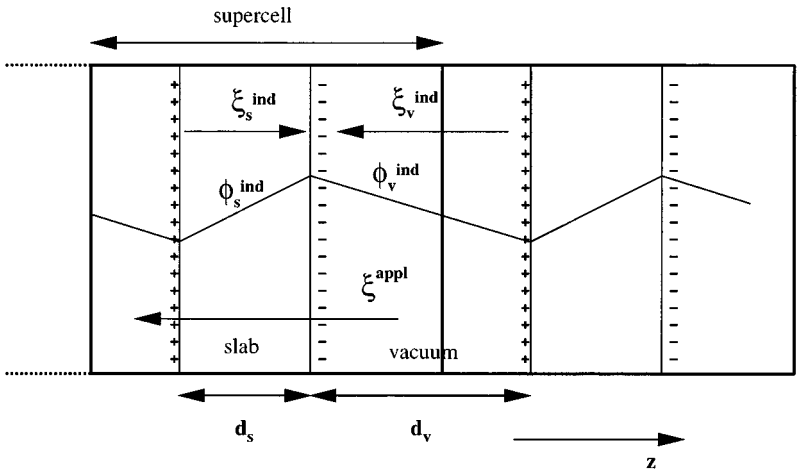

FIG. 10. Schematic representation of the periodic slabs with their surface charge densities due to the applied electric field ξ^{appl}. The corresponding induced electric fields in the slab ξ_s^{ind} and in the vacuum gap ξ_v^{ind} are also shown, along with the contributions ϕ_s^{ind} and ϕ_v^{ind} to the potential energy of an electron.

mation, a more detailed calculation of the tunneling current in presence of the electric field has to be performed. This is presented next.

D. Application to STM imaging

In order to determine the influence of the tip-induced electric field on the differential conductance values, we proceed in a similar way to that described previously (Sec. III C). The conductance is calculated via the expression of Eq. (4) using the eigenstates obtained in the presence of the electric field, and averaged over the same set of random localized initial states as in Sec. III C. The final state is still chosen to be a localized Gaussian state in the vacuum gap moving according to the scan direction. It should be mentioned that the presence of the tip is, in this case, partially taken into account by the presence of its induced electric field, which in turn polarizes the surface (as we have seen in the previous sections). Figure 9 represents a constant-current image of the surface unit cell. Constant current scans have been also determined for different current values (for example see Fig. 4 in Ref. 13). The ''tip-sample'' distances are larger than for the zero-field case (even for larger current values): this is to be expected because of the field-induced electron spreading into the vacuum. When the ''tip-sample'' distance is around or slightly above the turning point z_{tp} defined in the previous section, the molecule appears slightly below the clean dimer in the corresponding image. This contrast originates from the difference of the surface polarization above the molecule and the clean dimer. The electronic states respond more strongly to the electric field above the dimer than above the molecule. This effect is partially compensated by the fact that the molecule stands above the level of the rest of the surface. This explains why, in Fig. 4 in Ref. 13, the contrast is slightly inverted for smaller ''tip-sample'' distances (i.e., larger conductance values). Consequently we propose that under such conditions, the results we have obtained may explain the contrast observed experimentally in the STM images. We are not able to understand such a contrast by considering only surface wave functions obtained in zero electric field.

V. CONCLUSION

In this paper, we have studied the STM contrast of the Si(001) surface on which C_2H_4 molecules are adsorbed. In particular, we have been interested in the influence of the tip-induced electric field on such a contrast. The system is investigated by mean of an *ab initio* density functional method (projector augmented wave) combined with the Car-Parrinello scheme to achieve the ground-state atomic and electronic structures. We first showed that the experimental results, i.e., that the ethylene molecules appear slightly darker than the clean silicon dimer in the filled-state STM images, cannot be understood from calculations done with zero electric field. Consequently the tip-induced electric field and the corresponding modifications of the surface electronic structure must play an important role in the tunneling process. We have performed a detailed analysis of the polarization of the surface charge density with and without adsorbed ethylene molecules. It has been shown that in the presence of a tip-induced electric field directed towards the surface, the electronic states are spread into the vacuum as expected. However, the response to the electric field is found to be more important above the clean dimers than above the adsorbed molecules. This effect, combined with the particular surface topography (the molecules are lying above the rest of the surface), means that above a critical tip-sample distance, the clean dimers appear brighter than the molecules in constant-current scans in agreement with the experiments.

This result opens the way for further investigations of the role of electric fields in STM. We plan to extend our calculations to include the atomic structure of the tip, and hence other types of tip-sample interaction.

ACKNOWLEDGMENTS

We thank Dr. G.A.D. Briggs for a number of discussions about his STM experimental results and Dr. P.E. Blöchl for providing us with the original PAW code. We are grateful to the Engineering and Physical Science Research Council for support under Grant Nos. GR/J67734 and GR/K80495.

APPENDIX: SURFACE CHARGE DENSITY FOR A DIELECTRIC SLAB IN A SUPERCELL WITH PERIODIC BOUNDARY CONDITIONS

In this appendix, we relate the polarization charge density obtained with the PAW method to the classic surface charge density induced in a dielectric by an applied electric field

TABLE I. Values of the surface charge densities obtained from the *ab initio* calculation (σ_{calc}) and estimated from classical electrostatics (σ_{estim}) in electron/Å^2.

ξ^{appl} [eV/Å]	σ_{calc} [e^-/Å^2]	σ_{estim} [e^-/Å^2]	error [%]
-0.1029	9.29×10^{-4}	9.09×10^{-4}	2
-0.2057	1.87×10^{-3}	1.82×10^{-3}	3
-0.4114	3.81×10^{-3}	3.64×10^{-3}	5
-0.7714	7.82×10^{-3}	6.82×10^{-3}	15
-1.0285	1.17×10^{-2}	9.09×10^{-3}	29

using standard electrostatic formalism. Let us first consider an isolated slab of thickness d_s made of a dielectric material characterized by its dielectric constant or relative permittivity ϵ_r. An applied (external) electric field ξ^{appl} perpendicular to the slab surface induces charge displacements in the slab towards the surfaces which correspond to the induced electric field inside the slab ξ_s^{ind} (the so-called depolarization field). The relation between the applied field and the induced field, obtained form the boundary conditions at the slab surface, is $\xi_s^{\text{ind}}=(1-\epsilon_r)/\epsilon_r\xi^{\text{appl}}$. Since ϵ_r is always greater than unity, the induced field is opposite to the applied field as expected. Using Gauss's law, one finds the expression for the corresponding induced surface charge density σ,

$$|\sigma|=\frac{\epsilon_r-1}{\epsilon_r}|\xi^{\text{appl}}|\epsilon_0, \tag{A1}$$

which is a standard result of classical electrostatics ($\epsilon_0=8.85\times10^{-12}$ H/m is the permittivity of the vacuum).

However, in the present case, the periodic boundary conditions on the supercell in which the slab is located imply an electrostatic interaction between adjacent periodic slabs. The surface charge density of the periodic slabs generates a corresponding induced electric field ξ_v^{ind} in the vacuum gap as schematically represented in Fig. 10. Then, the boundary conditions for the electric fields at the separation surface between the slab and the vacuum is

$$\epsilon_r(\xi^{\text{appl}}+\xi_s^{\text{ind}})=\xi^{\text{appl}}+\xi_v^{\text{ind}}. \tag{A2}$$

Taking into account the periodic boundary conditions, we find that the continuity of the induced potential on the successive slab-vacuum separation surfaces can be recast as a ''conservation'' equation for the corresponding induced field,

$$d_s\xi_s^{\text{ind}}+d_v\xi_v^{\text{ind}}=0, \tag{A3}$$

where d_v is the length of the vacuum region in the supercell in the direction perpendicular to the slab surface (d_s+d_v being then the length of the supercell in this direction). Combining Eqs. (A2) and (A3) gives the expression for the induced field in the slab,

$$\xi_s^{\text{ind}}=\frac{1-\epsilon_r}{\epsilon_r+d_s/d_v}\xi^{\text{appl}}. \tag{A4}$$

Finally, one can define the induced surface density charge from the field flux passing through a surface element by $|\sigma|/\epsilon_0\equiv|(\xi^{\text{appl}}+\xi_s^{\text{ind}})-(\xi^{\text{appl}}+\xi_v^{\text{ind}})|$. This gives us the final expression of the induced surface density charge

$$|\sigma|=\frac{\epsilon_r-1}{\epsilon_r}\left[\frac{1+\delta}{1+\delta/\epsilon_r}\right]|\xi^{\text{appl}}|\epsilon_0, \tag{A5}$$

where $\delta=d_s/d_v$. It is worth noticing that Eq. (A5) is equivalent to Eq. (A1) if we replace the applied field by the effective applied field $\xi^{\text{eff}}=\xi^{\text{appl}}+\xi_v^{\text{ind}}=(1+\delta)/(1+\delta/\epsilon_r)\xi^{\text{appl}}=\alpha_{\text{cell}}\xi^{\text{appl}}$. The enhancing factor α_{cell} is always larger than unity and is dependent on the dimensions of the slab and of the supercell. In the case of an infinite vacuum region (i.e., an isolated single slab), $\delta\to0$ and one recovers Eq. (A1) from Eq. (A5). This means that the true effective values of the uniform tip-induced electric field are actually $\alpha_{\text{cell}}\xi^{\text{ext}}$.

Table I shows the values of the calculated surface charge density σ_{calc} from the integration (over the slab region) of the averaged polarization charge density $\langle\Delta\tilde{n}(z)\rangle_{xy}$ shown on Fig. 3, as well as the estimated surface charge density σ_{estim} from Eq. (A5) for the experimental silicon dielectric constant $\epsilon_r=12$. These values show a good agreement between the present *ab initio* calculations and simple classical electrostatics for the lowest values of the applied external field ξ^{ext}. The differences increase for larger ξ^{ext} values as the polarization becomes nonlinear in the applied field. For the biggest ξ^{ext} value, the presence of the artificially bound states in the potential well due to the cutoff function $f(z)$ distorts the results as previously mentioned in Sec. IV B.

[1] G. Binnig, H. Rohrer, C. Gerber, and E. Weibel, Phys. Rev. Lett. **49**, 57 (1982).

[2] R.J. Hamers, R.M. Tromp, and J.E. Demuth, Phys. Rev. Lett. **55**, 1303 (1985); R.M. Tromp, R.J. Hamers, and J.E. Demuth, Phys. Rev. B **34**, 5343 (1986); R.J. Hamers and U.K. Köhler, J. Vac. Sci. Technol. A **7**, 2854 (1989).

[3] A.J. Mayne, A.R. Avery, J. Knall, T.S. Jones, G.A.D. Briggs, and W.H. Weinberg, Surf. Sci. **284**, 247 (1993).

[4] A.J. Mayne, Ph.D. thesis, University of Oxford, 1994.

[5] J. Tersoff and D.R. Hamann, Phys. Rev. B **31**, 805 (1985).

[6] G. Doyen, D. Drakova, and M. Scheffler, Phys. Rev. B **47**, 9778 (1993).

[7] M.L. Bocquet and P. Sautet, Surf. Sci. **360**, 128 (1996).

[8] S.C. Lam and R.J. Needs, J. Phys. Condens. Matter **5**, 2101 (1993); Surf. Sci. **277**, 173 (1992).

[9] J. Neugebauer and M. Scheffler, Surf. Sci. **287-288**, 572 (1993); Phys. Rev. B **46**, 16 067 (1992).

[10] Z.H. Huang, M. Weimer, R.E. Allen, and H. Lim, J. Vac. Sci. Technol. A **10**, 974 (1992).

[11] K. Hirose and M. Tsukada, Phys. Rev. Lett. **73**, 150 (1994); Phys. Rev. B **51**, 5278 (1995).

[12] N. Kobayashi, K. Hirose, and M. Tsukada, Jpn. J. Appl. Phys. **35**, 3710 (1996).

[13] H. Ness, A.J. Fisher, and G.A.D. Briggs, Surf. Sci. Lett. (to be published).

[14] P.E. Blöchl, Phys. Rev. B **50**, 17 953 (1994).

[15] P.E. Blöchl, Phys. Rev. B **41**, 5414 (1990).

[16] D. Vanderbilt, Phys. Rev. B **41**, 7892 (1990).

[17] K. Laasonen, A. Pasquarello, R. Car, C. Lee, and D. Vanderbilt, Phys. Rev. B **47**, 10 142 (1993).
[18] W. Kohn and L.J. Sham, Phys. Rev. **140**, A1133 (1965).
[19] P.C. Hohenberg and W. Kohn, Phys. Rev. **136**, B684 (1964).
[20] J.P. Perdew and A. Zunger, Phys. Rev. B **23**, 5048 (1981).
[21] D.M. Ceperley and B.J. Alder, Phys. Rev. Lett. **45**, 566 (1980).
[22] R. Car and M. Parrinello, Phys. Rev. Lett. **55**, 2471 (1985); in *Simple Molecular Systems at Very High Density*, edited by A. Polian (Plenum, New York, 1988), p. 455.
[23] Z. Zhu, N. Shima, and M. Tsukada, Phys. Rev. B **40**, 11 868 (1989); N. Roberts and R.J. Needs, Surf. Sci. **236**, 112 (1990); S. Tang, A.J. Freeman, and B. Delley, Phys. Rev. B **45**, 1776 (1992).
[24] J. Dabrowski and M. Scheffler, Appl. Surf. Sci. **56-58**, 15 (1992).
[25] A.J. Fisher, P.E. Blöchl, and G.A.D. Briggs, Surf. Sci. **374**, 298 (1997).
[26] L. Clemen, R.M. Wallace, P.A. Taylor, W.J. Choyke, M.J. Dresser, W.H. Weinberg, and J.T. Yates, Jr., Surf. Sci. **268**, 205 (1992).
[27] A.J. Fisher and P.E. Blöchl, in *Computations for the Nano-Scale*, Vol. 240 of *NATO Advanced Study Institute, Series E: Applied Sciences*, edited by P.E. Blöchl *et al.* (Kluwer, Dordrecht, 1993), p. 185.
[28] G.Doyen, in *Scanning Tunneling Microscopy III*, Vol. 29 of *Springer Series in Surface Science*, edited by R. Wiesendanger and H.J. Güntherodt (Springer-Verlag, Berlin, 1993), p. 23.
[29] T.N. Todorov, G.A.D. Briggs, and A.P. Sutton, J. Phys. Condens. Matter **5**, 2389 (1993); J.B. Pendry, A.B. Prêtre, and B.C.H. Krutzen, J. Phys. Condens. Matter **3**, 4313 (1991); C. Joachim and P. Sautet, in *Scanning Tunneling Microscopy and Related Methods*, Vol. 184 of *NATO Advanced Study Institute, Series E: Applied Sciences*, edited by R.J. Behm *et al.* (Kluwer, Dordrecht, 1990), p. 377.
[30] N.W. Ashcroft and N.D. Mermin, in *Solid State Physics*, International ed. (Saunders, Philadelphia, 1976), p. 553.
[31] *Handbook of Chemistry and Physics*, edited by D.R. Lide (CRC, Boca Raton, FL, 1994), pp. 6–155.
[32] C.G. Van de Walle and P.E. Blöchl, Phys. Rev. B **47**, 4244 (1993).
[33] P. Pulay, Mol. Phys. **17**, 197 (1969).
[34] M.M.D. Ramos, A.M. Stoneham, and A.P. Sutton, J. Phys. Condens. Matter **5**, 2849 (1993).
[35] P. Badziag, W.S. Verwoerd, and M.A. Van Hove, Phys. Rev. B **43**, 2058 (1991).
[36] R. Maboudian, K. Pond, V. Bresslerhill, M. Wassermeier, P.M. Petroff, G.A.D. Briggs, and W.H. Weinberg, Surf. Sci. Lett. **275**, L662 (1992).
[37] M. McEllistrem, G. Haase, D. Chen, and R.J. Hamers, Phys. Rev. Lett. **70**, 2471 (1993).